ESPL
Earth Surface Processes and Landforms

Introduction

Weathering and erosion of sandstone produces a great variety of natural landforms (Young *et al.*, 2009). Some of the finest ancient monuments are carved in sandstone (e.g. Petra, Jordan, Heinrichs, 2008), and sandstone is also one of the most frequently used dimension stones (Siegesmund and Snethlage, 2011). Thus, understanding the weathering and erosion of sandstone is crucial in the preservation of unique natural landforms as well as in protecting ancient monuments. However, those factors affecting sandstone weathering and erosion are still not well understood, especially on the field scale as the following authors demonstrate on numerous examples (Viles, 2001, 2013; Turkington and Paradise, 2005; Warke *et al.*, 2006; Ruedrich and Siegesmund, 2007; Mol, 2014).

Salt and frost weathering are probably the most common processes responsible for sandstone degradation on bare sandstone surfaces (Steiger *et al.*, 2011). This is nicely demonstrated by Huinink *et al.* (2004) showing that the location where salt weathering will occur is controlled by the moisture flux, and hence by the hydraulic field and its boundary conditions. Mol and Viles (2012) documented a dynamic relationship between surface hardness (i.e. case hardening), degree of weathering, and internal moisture regimes. Laboratory experiments on sandstone specimens several centimeters in size, make it possible to compare the durability of various sandstone types to a specific salt, to frost weathering, or to test the degree of damage created by various salts to a single sandstone lithology (Robinson and Williams, 2000; Williams and Robinson, 2001). However, these experiments are on too small a scale and too simplified to account for effects of the hydraulic field and other factors occurring on the field scale. Also, moisture content and other conditions used in laboratory tests are often far from the conditions present in the field (Dorn *et al.*, 2013).

As has recently been shown by laboratory experiments performed on many different sandstone types and under controlled conditions, increased gravity-induced stress (hereafter 'stress') significantly decreases the salt and frost weathering rate (Bruthans *et al.*, 2014; Rihosek *et al.*, 2016). Via physical modeling it was also demonstrated that stress plays a crucial role in the origin of natural sandstone landforms such as pillars, arches, alcoves, and pedestal rocks. Numerical modeling revealed how erosion and weathering are coordinated by the stress field to reshape the original rock exposure geometry into

a new one, where portions with low loading have been removed (Bruthans *et al.*, 2014). Nevertheless, it is still difficult to carry out a relevant quantitative study of those factors affecting the weathering and erosion rates in the field for the following specific reasons: Erosion is too slow to be measured over the same time period as those factors affecting it. Contrast in weathering intensity at a single locality is too small to see clear differences in erosion rates. Too many weathering factors occur at a single location and/or during the same time period. Finally, lithology changes on the same scale as the weathering factors, such that the effects of weathering and lithology on the erosion rate can not be separated.

That is why the present study is focused upon a unique sandstone overhang with extremely high erosion rates (Figures 1A–1D, 2A, and 2B). During the last ~35 years, the fallen material has gradually accumulated below the overhang, forming a 1.8 m high pile (mean debris accumulation rate of approximately 50 mm/yr; time period reported by a local resident). Such rapid sandstone erosion only occurs in this overhang, the only wet place in the studied sandstone cliff. The source of the moisture at the overhang is suspected to be a leak from a sewerage reservoir (Figure 1B). No other segments of the sandstone cliff (including other overhangs) show traces of such rapid erosion. A well-preserved engraving '1915', which was found just 5 m to the west of the overhang in the same sandstone layer (Figure 2C), demonstrates that the erosion rate does not exceed 1 mm/100 yr on dry surfaces.

The erosion rate at the seasonally wet overhang is at least 2000 times faster.

We consider this overhang as an appropriate field-scale and decade-long 'model', which may facilitate an understanding of rapid sandstone weathering and erosion under real conditions, in general. As the rapid decay of sandstone in this locality is confined to a limited place with neighboring stable sandstone, the properties of both environments can be compared.

The purpose of this study was to characterize those factors responsible for the rapid weathering and erosion of the sandstone in the overhang in contrast to the stable sandstone in its immediate surroundings and use this knowledge to interpret relative rate of erosion of overhangs in the past in Central Europe and elsewhere. To attain this, the following particular tasks were carried out:

- sandstone and salt efflorescence were characterized from the mineralogical point of view and the salt content was determined;
- erosion rates were measured – at various locations in the overhang, and the conditions under which the erosion rates were maximal and minimal were analyzed;
- selected parameters including, tensile strength, moisture, suction and water chemistry were monitored in the overhang and its vicinity;
- the field data were complemented with a laboratory simulation of frost weathering of the sandstone, and numerical modeling of the stress in the studied overhang.
- erosion rates measured in the artificially wetted overhang were compared with those derived for overhangs with ambient moisture content in Central Europe and Colorado

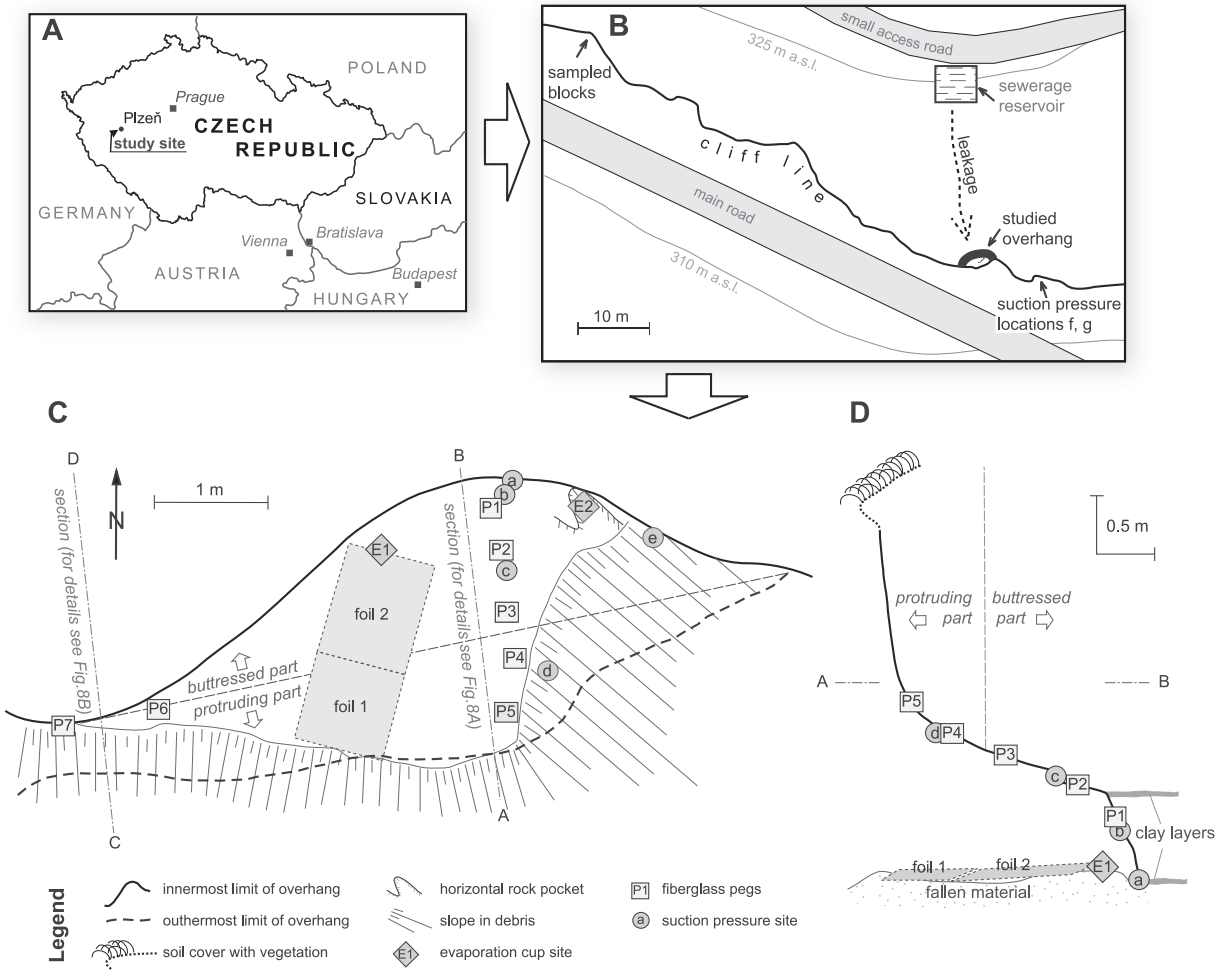

Figure 1. Overall situation of the studied overhang: (A) location in Europe; (B) study area; (C) plan of the studied overhang, with positions of particular sites; for details about the sections A–B and C–D see Figures 8A and 8B; (D) vertical section by the overhang.

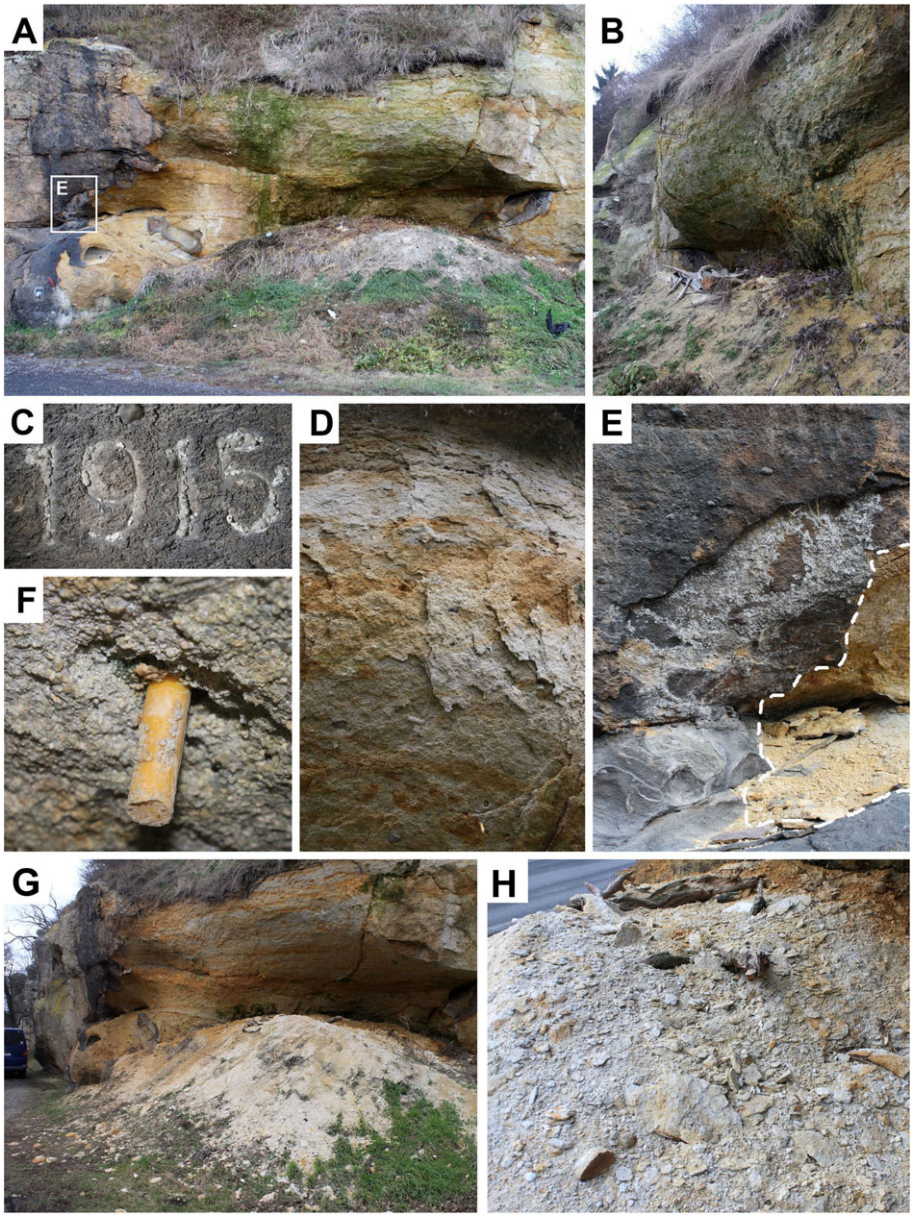

Figure 2. Field situation of the overhang and nearby surroundings: (A) front view of the overhang with the heap of fallen materials (photograph taken prior to first freezing – December 2011) – note the vegetation cover at the heap top; (B) side view; (C) well-preserved engraving '1915' situated 5 m to the west of the overhang; (D) flakes parallel to overhang surface; (E) detail from part A showing case hardening covered by salt efflorescence outside of the studied overhang area (left from the dashed line); (F) fiberglass pegs for measurement of erosion rate; (G) stable cliff wall with case hardening (left in the photograph), and front side view of the overhang with heap covered by freshly fallen material – March 2013); (H) accumulation of flakes and sand on the top of the heap. [Colour figure can be viewed at wileyonlinelibrary.com]

Plateau (USA) and used to develop ideas on the timing of evolution of these overhangs.

Characteristics of the Study Area

The studied overhang developed in a sandstone cliff named 'Čertova Kazatelna' ('Devil's Pulpit' in English), and is situated 85 km west-southwest (WSW) of Prague in the western part of the town of Plzeň, at an altitude of 315 m above sea level (a.s.l.) (Figures 1A and 1B). The mean annual precipitation in the area is 527 mm, with an average temperature of 7.5 °C (Station Plzeň-Bolevec, 1961–1990). The mean regional evapotranspiration is ~90% (according to the Czech Hydrometerological Institute).

The cliff is approximately 700 m long and up to 22 m high, and it lines the alluvium of the Mže River (Vítek, 1987). The cliff is formed by arkosic sandstone and conglomerate that belong to the upper part of Nýřany member of the Kladno formation, which is of Carboniferous age. The material of the cliff is fluvial in origin, with common cross-bedding (Opluštil *et al.*, 2005), belonging to the Plzeň Basin, one of the post-Variscan intermountain depressions, with a several hundred meter thick infill. The sediments are faulted but not folded, the beds are subhorizontal. The cliff hosts several overhangs, numerous tafoni-like forms, and honeycombs (Vítek, 1987).

The easternmost part of the cliff, in close proximity to the overhang, is studied; it is located at 49°45′28.1″N, 13°20′24.3″E (Figure 1B). Here, the cliff is from 6 to 10 m high. The studied overhang, approximately 3 m wide and up to 1.5 m deep, is situated at the base of the cliff (Figures 1C, 2A, and 2B). The overhang faces southward. Its sides and ceiling are made of coarse sandstone and conglomerate, with sporadic pebbles up to 5 cm in size. Two thin (~1 cm) clay horizons

cause abrupt changes in the ceiling geometry (Figure 1D). The overhang's sides and ceiling are decaying into flakes from several millimeters up to several tens of millimeters thick, similar to those described by Dragovich (1967). Flakes are parallel to the overhang surface (Figure 2D). The pile below the overhang has formed by the accumulation of fallen flakes. Outside the area of the studied overhang, the sandstone exposures are mostly covered by case hardening 5–16 mm thick (Figure 2E). Relics of the case hardening in some parts of the overhang indicate that the case hardening originally occurred there, as well. Salt efflorescences are common on sandstone exposures shielded from the rain; by contrast, they occur only temporarily on the studied overhang. In the colder periods of the year, water drips from the western part of the overhang.

Materials and Methods

Solid sampling and sample treatment

Solid samples were taken from the overhang, and also from other parts of the cliff; i.e. from a sandstone outcrop unaffected by seeping moisture. For the locations of the sampling sites see Figures 1C and 1D. Samples 5 mm thick (approximately 5–20 g of material) were scraped off from the surface zone of the overhang. This material was used for solid phase identification, as well as periodic determination of moisture and salt contents. Samples were taken from the wider surroundings of fiberglass pegs (Figure 2F) in order to not affect the erosion rates. Additionally, materials that fell onto plastic foil were sampled for a mineralogical study and measurements of their tensile strength. Sandstone blocks sampled outside the overhang area from the same lithological horizon were used as background for both the tensile strength measurements and frost weathering tests.

Phase identification and salt content

To determine the mineralogical composition of the matrix in the sandstone cliff, the fine clay- and silt-fraction was separated by sedimentation of the disintegrated flakes in distilled water. Phase identification was determined by conventional X-ray diffraction (XRD) analyses using a PANalytical X'Pert Pro diffractometer under the following conditions: CuKα radiation 40 kV, 30 mA, step scanning at 0.013°/300 s in the range 2°–89° 2θ. Qualitative analysis was performed using the HighScorePlus software package (PANalytical, the Netherlands; HighScorePlus, 2011), Diffrac-Plus software package (Bruker AXS, Germany), and JCPDS PDF-2 database (2004).

To determine the salt content, the solid material was dried at 105 °C until a stable weight was obtained, crushed by a rubber pestle, and quartered. A small amount of material was mixed with deionized water (1:100), shaken at 150 RPM for 24 hours, filtered through a membrane filter (Millipore®), and stored in HDPE bottles in the cold. The conductivity of leachates was measured, and TDS (total dissolved solids) was calculated from the electric conductivity of the leachate based on a calibration using the chemical composition of the analyzed leachates.

Measurement of erosion rate

Two different approaches were applied to measure the erosion rate of the sandstone overhang. The first approach consisted of placing the plastic foil on the floor below the overhang ceiling, and collecting the fallen material during several time periods (Figures 1C and 1D). The fallen material was dried, weighed, and its weight was divided by the surface area of the plastic foil, and by the time period for which material was collected (in $kg/m^2/day$). Finally, the erosion rate was calculated from the accumulation rate using the following equation:

$$RR = AR/dens*AC_{area}/EX_{area},$$

where RR is the erosion rate (in m/day); AR is the accumulation rate (in $kg/m^2/day$); dens is sandstone density (in kg/m^3); AC_{area} is the extent of the accumulation area (in m^2); EX_{area} is the extent of the exposure area (in m^2).

Between 2008 and 2011, the rate was occasionally measured in 0.2–1 day long periods during different seasons of the year. Between December 26, 2012 and March 14, 2015 the erosion rate was measured continuously in 1–3 month long periods.

The second approach was based on placing fiberglass pegs (0.8 cm in diameter, ~15 cm long, Figure 2F) into drill holes in the sandstone, fixing them with epoxy resin, and measuring the distance between the peg top and the rock surface in the peg's surroundings with a caliper. Five fiberglass pegs (P1–P5) were emplaced into the overhang on March 3, 2013, forming a line from the innermost part of the overhang outwards (Figures 1C and 1D). Two additional pegs (P6 and P7) were placed on December 2, 2013 on the vertical wall west of the overhang. Surface erosion around the fiberglass pegs was measured in 1–3 months long periods. Due to the undulating surface, the distance between the peg top and rock surface is measured with a precision of ±2 mm.

Sandstone bulk density was measured on small samples by the wax immersion method (ASTM, 2004). The bulk density of debris which had accumulated in a pile below the overhang was measured as the ratio of the weight of debris taken from a hole dug into the debris pile, divided by the volume of the hole. The hole bottom and sides were covered by thin plastic foil, and the volume of the excavated material was measured by the amount of liquid needed to fill the hole.

Erosion rates were compared with air temperatures measured hourly at the Plzeň Mikulka station (Czech Hydrometeorological Institute, situated 3 km east of the overhang, altitude of 370 m a.s.l.). Total duration of freezing was calculated for each period. As a second parameter, those continuous freezing periods exceeding 24 hours were selected, and their duration was multiplied by the mean temperature during the period. Resulting numbers were summed over each monitoring period. This parameter, called FDI ($^oC \times day$) later in the text, accounts for both the duration and intensity of freezing.

Tensile strength measurement

Cementation cohesion of sandstone can be roughly approximated by the tensile strength (Bruthans *et al.*, 2012b, 2014). The tensile strength is an important property showing resistance of sandstone to disruptive impact of majority of weathering and erosion processes (Steiger and Asmussen, 2008; Goudie, 2013). The tensile strength of dry and water saturated samples was measured in the laboratory. Strips of T profile (aluminum with a 2 by 2 cm surface area) were glued with epoxy to the sandstone surfaces. After hardening, a tensile force was gradually increased perpendicular to the sandstone surface until the sandstone beneath the epoxy failed. The maximum (pull off) force and effective area was measured (tensiometer) and calculated in kPa (Bruthans *et al.*, 2014). The dry tensile strength was measured after drying the sample under laboratory conditions (25 °C, 50% relative humidity). The saturated tensile strength was measured by placing the sandstone blocks in a water tank

(with the surface measured facing upward). The block was slowly saturated adding water, and the tensile strength was measured after one week of saturation.

Determination of moisture content and drip water/leachate chemistry

Moisture content is a key factor in many processes of weathering and deterioration affecting sandstones (Viles and Goudie, 2007; Mol and Viles, 2010). Moisture content in the overhang subsurface was measured by the gravimetric method. The material was weighed in the field, dried at 105 °C, and weighed again until a stable weight was reached. As the surface of sandstone outside of the region of the overhang is firm, and collecting samples would thus result in unacceptable damage; the moisture content outside of the area of the overhang was monitored indirectly by suction, and thus its relationship with moisture content. To monitor the suction, the miniature tensiometer T5x (UMS Germany) was used. The T5x device is designed to measure the capillary suction in soils and other porous materials. The more negative the suction, the lower the water content (Tindall and Kunkel, 1999). Suction was measured in drilled holes 5 mm in diameter at depths 20–40 mm below the sandstone surface. The position of the measuring points are labeled as a–g in Figures 1C and 1D. The holes were sealed by plastic foil between individual measurements to prevent evaporation.

The air temperature and humidity was monitored by sensor with a datalogger placed inside the overhang between March 3, 2013 and October 5, 2014. The potential evaporation rate was measured by two plastic cups, 57 mm in diameter, filled by distilled water, and weighed periodically (E1, E2 in Figures 1C and 1D). The evaporation surface was protected with a mesh, 2 mm in diameter, to prevent damage by animals.

The chemical composition of the liquid samples (dripping water, local spring water, and solid-water leachates) were analyzed for concentrations of nitrates, chlorides, and sulfates by high performance liquid chromatography (HPLC) (Dionex ICS-2000); cations by inductively coupled plasma optical emission spectrometry (ICP OES) (Thermo Scientific) in the laboratories of the Institute of Geology of The Czech Academy of Sciences and the Faculty of Science, Charles University.

Laboratory frost weathering tests

Frost weathering tests were performed to evaluate the effect of gravity-induced stress on frost weathering rate. Sandstone cubes with edge lengths of 40 ± 1 mm were cut from a block of the collected sandstone using a diamond saw cooled by water. Susceptibility to frost weathering was tested by repeated cycles consisting of submerging the cubes in water (+20 °C) for ≥8 hours, followed by placing them in a freezer (−20 °C) for the same period of time. To remove the loose grains, the cubes were turned upside-down each 10th cycle for 10 seconds and submerged again into the water. The cubes were weighed in each cycle.

Frost weathering tests were done with three unconfined and three uniaxially loaded cubes. Unconfined cubes were left bare, touching the base on its lower side. Uniaxially loaded cubes were compressed by placing square stiff steel plates of the same size as the cube sides onto the opposite side of the cube. The plates were compressed against the cube sides by tightening the nuts on a steel casing constructed around the cube. The nuts were tightened by a torque screwdriver to 0.75 Nm, which corresponds to a confinement of ~680 kPa, based on calibration with a tensiometer.

Numerical modeling

Numerical modeling was used to predict stress distribution within the rock mass of the overhang and its effect on the erosion rate. PLAXIS 3D geotechnical software was used. Model dimensions were exactly the same as the dimensions of the overhang, and the model geometry closely resembled the geometry of the physical models. The three-dimensional (3D) shape of the overhang was created by means of photogrammetry. The finite element mesh of the model consisted of 618 000 tetrahedral finite elements with second-order interpolation of displacements. Boundary displacements were assigned for the bottom boundary, zero horizontal displacement in the normal direction to boundary planes (free displacement in the other two axes) for left and right vertical model boundaries with the rock mass, fixed horizontal displacement (free vertical displacement) for the back vertical boundary with the rock mass, and free displacement in all three axes for the free superficial boundary (frontal and upper boundary).

The sandstone was described using a Mohr–Coulomb constitutive model. Model parameters for weak sandstones were used: Young modulus of $E = 4$ GPa, Poisson's ratio nu =0.3, internal friction angle $\phi = 30°$, angle of dilatancy was estimated as $\psi = 15°$, cohesion =600 kPa, density as $\rho = 2390$ (wet) kg/m^3. The stress state within the physical model was generated using the gravity loading procedure available in the PLAXIS 3D software. Stress was generated during finite element simulation. The initial stress was prescribed as zero alongside of zero gravity acceleration. During the stress generation stage, the gravity acceleration was gradually increased to the value of $g = 9.81$ m/s^2 under the condition of constant density.

Results and Discussion

Solid phase characterization and salt content

The fine fraction (silt and clay) of the sandstone, separated from the overhang material, is formed of quartz, kaolinite, illite, and K-feldspar. Dark surficial case hardening zone contains a significant portion of gypsum and most probably also organic matter and trapped dust particles (Gorbushina, 2007, and references cited therein). Gypsum is also the major constituent of all the efflorescence samples analyzed. Occurrence of efflorescence is strongly connected to those parts of the case hardening situated outside of the overhang area in those places shielded from rain. By contrast, in the overhang itself, the efflorescence is only present temporarily, due to the fast erosion of the material.

The measured salt content in the overhang samples varied noticeably during the year between 0.1 and 2 wt% in depths from 0 to 5 mm (Figure 3A). The salt content abruptly decreased during November, as the overhang became wet, and salts were dissolved and leached by seeping water (Figure 3A). Salts started to accumulate in spring, and reached its maximum content either in summer or in autumn, depending on the time when pore water ceased to flow towards the sandstone surface at a specific part of the overhang. Flakes which fell from the overhang during the winter showed only low content of salts (0.06–0.1 wt%).

A tight correlation was found between the concentration of sulfate and calcium ($R^2 = 0.88$), sulfate and magnesium ($R^2 = 0.87$), sodium with both chlorides ($R^2 = 0.67$), and nitrates ($R^2 = 0.63$) in leachates from the overhang. Gypsum was

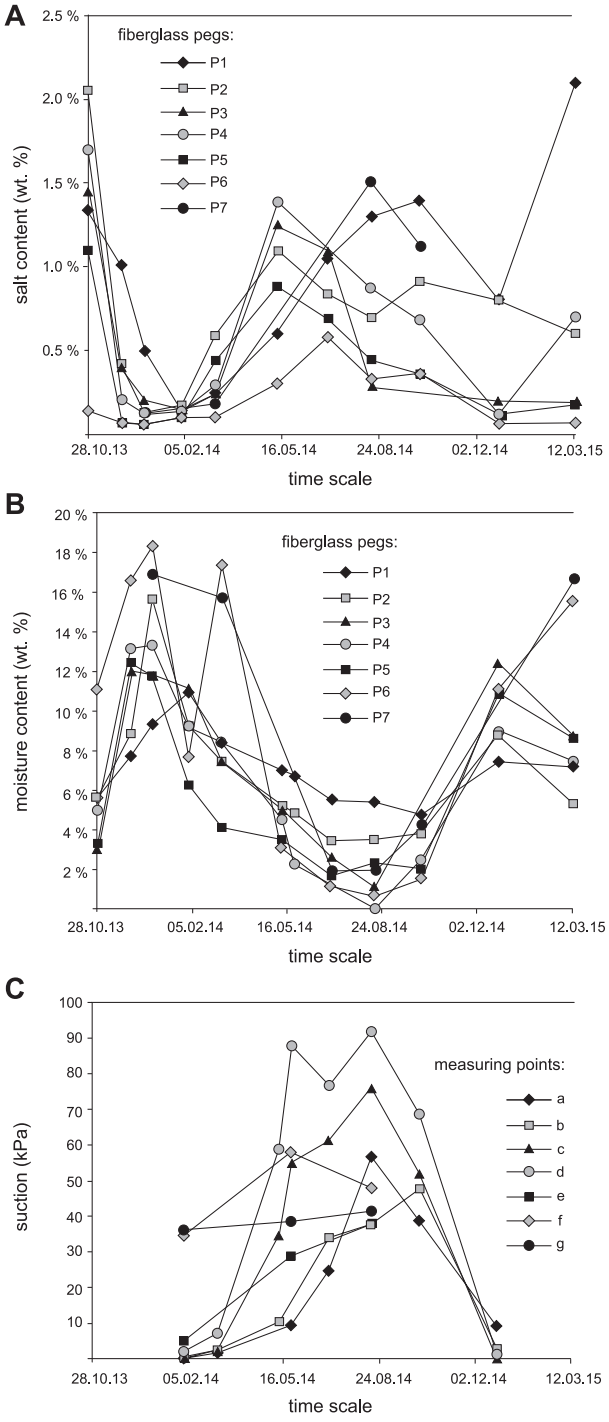

Figure 3. Temporal changes of moisture and salt content in overhang: (A) salt content; (B) moisture content; (C) suction.

identified as the main dissoluble mineral based on the ionic composition of the leachates. Mean gypsum content in the leachates is ~40% of dissoluble matter. Other potentially occurring minerals are nitratine ($NaNO_3$) and halite, with the mean content in the leachates of about 20 and 10%, respectively. Unlike gypsum, halite and nitratine were not confirmed by XRD. Both of these phases, especially the unstable nitratine, may only occur intermittently during the warmest periods of the day, since the increasing air moisture will dissolve such phases.

Erosion rate of sandstone in the overhang

Seven short-term measurements (0.2–1 day long) of the accumulation rate of the fallen materials from the overhang were made between 2008 and 2011. The maximum measured accumulation rate (60–200 g/m^2/day) occurred in the winter during an intense thaw (Table I, Figures 2G and 2H). Sandstone flakes were falling with a frequency of one every several seconds when the overhang was exposed to direct solar radiation. The peak intensity of the accumulation rate was estimated to be 5000 g/m^2/day (December 26, 2008). This event lasted just a few hours, but removed a considerable amount of weak material from the overhang's ceiling and walls. A much lower accumulation rate was measured when the air temperature was slightly below the freezing point (10–20 g/m^2/day). A negligible accumulation rate was measured prior to the first freezing (< 1 g/m^2/day). In spring and summer, the accumulation rate was low (2–10 g/m^2/day).

Between December 26, 2012 and March 14, 2015 the erosion rate was continuously measured in periods 1–3 months long. Within this period, three different winters occurred. Winter 2012/2013 was unusually long and cold, with freezing periods lasting 68 days in total. The longest continuous freezing period lasted 15 days. In contrast, winters 2013/2014 and 2014/2015 were mild, with freezing periods lasting a total of 34 and 27 days, respectively. The mean accumulation rate was extremely high during a cold winter (1047 g/m^2/day), while during a mild winters the mean accumulation rate was only 55–89 g/m^2/day (Table II). In spring, summer, and autumn the mean accumulation rate did not exceed 8 g/m^2/day. Erosion rate timings, measured on the fiberglass pegs, correspond to the accumulation rates of materials on the plastic foil. The highest erosion was observed between March 3, 2013 and April 11, 2013 (Table III). The erosion rate in 2013–2015, normalized to one year, was lowest in the inner part of the overhang (P1 and P2, with a rate of 3 to 4 mm/yr), but increasing outwards to 31 mm/yr at P5.

All the measurements clearly demonstrated that 87–99% of the material is accumulated during the winter period, and that its' falling is connected to the thaw after freezing periods. A

Table I. Accumulation and erosion rates based on materials collected on plastic foils over short time periods

Start time of accumulation rate measurement	Period of measurement (days)	Accumulation area (m^2)	Accumulation rate (g/m^2/day)	Climatic conditions
December 23, 2009 16:10	1.0	2.6	214	Cloudy, +3 °C; 24 hours after onset of thaw
December 25, 2010 14:00	0.9	4.5	62	Freezing in shade, but melting on insolated places
December 26, 2008 18:00	0.6	4.8	17	Cloudy; −1 °C
August 15, 2009 10:00	1.0	5.1	11	Clear sky, 25 °C
December 27, 2008 09:00	0.2	4.8	10	Cloudy; −1 °C
May 1, 2009 12:00	1.0	5.0	2.1	—
December 24, 2011 12:00	1.0	5.0	0.1	5 °C, no freezing yet

Table II. Accumulation and erosion rates based on materials collected on plastic foils over long time periods

Period	From	To	Foil 1 (g/m^2/day)	Foil 1, mean (g/m^2/day)	Erosion rate foil 1 (mm/yr)	Foil 2 (g/m^2/day)
Cold winter	December 26, 2012	March 3, 2013	1070		93	—
	March 3, 2013	April 11, 2013	1020	1047	88	—
Warmer period	April 11, 2013	May 21, 2013	<26		<2.3	—
	May 21, 2013	July 8, 2013	<4		<0.3	—
	July 8, 2013	August 22, 2013	0		0	—
	August 22, 2013	October 28, 2013	1.2	<8	0.1	—
Mild winter	October 28, 2013	December 2, 2013	39		3.4	—
	December 2, 2013	December 25, 2013	24		2.1	8
	December 25, 2013	February 1, 2014	103		8.9	90
	February 1, 2014	March 8, 2014	54	55	4.7	54
Warmer period	March 8, 2014	May 11, 2014	0		0	0
	May 11, 2014	July 2, 2014	0		0	0
	July 2, 2014	August 16, 2014	26		2.3	1.6
	August 16, 2014	October 5, 2014	0	7	0	0
Mild winter	October 5, 2014	December 25, 2014	11		0.9	2.3
	December 25, 2014	March 14, 2015	168	89	14	146
Mean December 26, 2012–December 25, 2013			315		27	
Mean December 26, 2013 – December 25, 2014			22		1.8	
Mean December 26, 2012–December 25, 2014			169		14	

Table III. Erosion in given time period (in millimeters), and in the last row the average erosion rate (in mm/yr) measured at the plastic pegs

Period	From	To	Freeze duration (days)	FDI (°C × day)	P1	P2	P3	P4	P5	P6[b]	P7[b]
Cold winter	March 3, 2013	April 11, 2013	17 (68[a])	–37 (–167[a])	3	2	10	26	47	—	—
Warmer period	April 11, 2013	October 28, 2013	0	0	≤2	≤2	≤2	≤2	≤2	—	—
Mild winter	October 28, 2013	March 8, 2014	34	–34	3	≤2	≤2	≤2	≤2	≤2	≤2
Warmer period	March 8, 2014	October 5, 2014	2	0	≤2	≤2	≤2	≤2	≤2	≤2	≤2
Mild winter	October 5, 2014	March 14, 2015	27	–35	≤2	≤2	19	≤2	16	≤2	≤2
Total	March 3, 2013	March 14, 2015	81	–106	8	7	34	26	63	≤2	≤2
Normalized to one year			40	–53	4	3	17	13	31	≤2	≤2

Note: FDI, factor of frost duration and intensity.
[a]Entire winter.
[b]Placed December 2, 2013.

cold winter with long freezing periods produces ~10 times more accumulated material than a mild winter with limited freezing (Table II). Considering the sandstone dry density of 2.3 g/cm^3, and average accumulation rate of 169 g/m^2/day, the mean erosion rate of the protruding part of the sandstone exposure is 14 mm/yr (Table II). However, at P6 and P7, where no protruding sandstone mass occurs, the erosion rate did not exceed 2 mm/yr (Table III).

The density of the debris pile below the overhang is 1.6 g/cm^3. As the original sandstone density is 2.3 g/cm^3, the 1.8 m high pile of debris was derived from a 1.25 m thick zone of sandstone. Thus the sandstone in the overhang has been eroded at a mean rate of 36 mm/yr over a period of 35 years. The long-term erosion rate is 2.6 times higher than the rate measured on foil 1 during 2013–2015, which is in agreement with the statement of a local resident that in the past the erosion rate was even greater.

The measured erosion rate is much higher than the reported erosion rates on sandstone exposures from various locations: 0.6–9 mm/yr in different coastal areas (Gill, 1981; Mottershead, 1994; Sunamura, 1996), 0–0.35 mm/yr in an arid climate measured on the sandstone tombs at the Petra Monument (Paradise, 2005; Heinrichs, 2008), or approximately 0.3 mm mm/yr in a mountainous precipitation-rich area of Japan (Imaizumi *et al.*, 2015).

Tensile strength

Tensile strength was measured on larger sandstone flakes having fallen from the overhang during the winter (Table IV). Most of the measurements were done on the flat sides of the flakes (A flakes); other measurements were also done in a direction perpendicular to the flat sides of the flakes (B flakes). A large sandstone block sampled outside of overhang area was measured to determine whether the materials of the flakes are weakened compared to the sandstone in the vicinity of the overhang. Results showed that the mean dry tensile strengths of both flakes and block are relatively low (120–270 kPa).

Table IV. Tensile strength of sandstone in overhang (flakes), and outside of the overhang area (block)

Surface type	Tensile strength	Mean value (kPa)	SD (kPa)	*n*
Sandstone block	Dry	266	28	9
Flakes A	Dry	194	105	17
Flakes B	Dry	122	38	14
Flakes A	Saturated	27	20	9

Note: *n*, number of measurements; SD, standard deviation.

Flakes A showed nearly the same dry tensile strengths as the sandstone block, while flakes B had dry tensile strengths only 50% of flakes A. A drastic decrease of tensile strength was observed when the material was saturated. The mean saturated tensile strength of flakes A dropped to 27 kPa, which is nearly one order of magnitude less than the same material under dry conditions (Table IV).

Moisture content and drip water chemistry

Rock moisture content in the overhang subsurface (0–5 mm depth) varies over time. The highest values (12–18 wt%) were measured in winter, while values of 1–5 wt% were measured during late spring and summer. High moisture values in winter correspond well with water dripping from the overhang ceiling and the presence of icicles when the temperature falls below zero. The largest variations in moisture content were determined in the outer parts of the overhang (spots P6, P7); and lowest in the innermost part (P1). This probably can be explained by differential evaporation rates in the two parts (Figure 3B).

High variations of the moisture content at a depth of 20 to 40 mm below the sandstone surface of the overhang are visible in the oscillation of the suction data (Figure 3C). The suction in the overhang was close to zero during winter, proving that the pore space was nearly fully saturated with water. As evaporation dominated during the summer, moisture was lost from the pore spaces, and suction reached up to 90 kPa in the outer parts of the overhang (Figure 3C, point d). In the inner part of overhang, the suction reaches between 40 and 60 kPa in summer (Figure 3C, points a and b). Suction measured outside the overhang area clearly showed low moisture content in the pore space in winter (35–45 kPa). Variation of the suction was much lower outside the overhang area. Based on the relationship between moisture content and suction, a moisture content of 40 kPa occurring in the winter outside of the overhang area is equal to a moisture content of ~5wt%. (Figure 4).

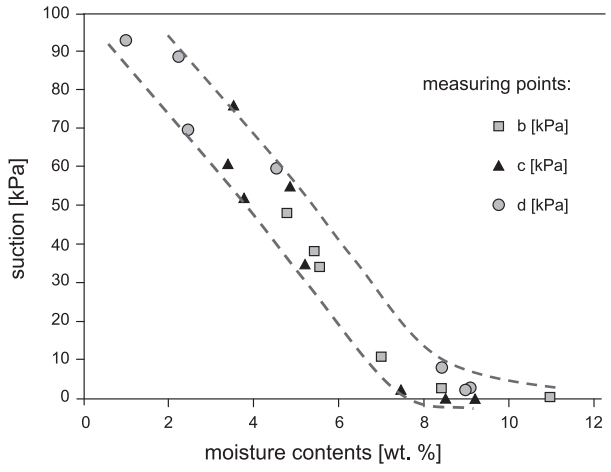

Figure 4. Relationship between moisture content and suction obtained from the overhang. The measured data fall within the region between the dashed lines.

The mean potential evaporation rate in the innermost part of the overhang is up to 13 mm/month in late spring and early summer, and about ~5 mm/month in late autumn and winter (mean annual rate ~ 6–7 mm/month), based on plastic cups with water (Table V). In the outer parts of the overhang, the evaporation rate will be considerably higher. The mean annual air temperature and relative humidity at the overhang is 11.6 °C and 78%, respectively.

Drip water in the western side of the overhang was sampled in 2009, 2011, and 2015. TDS were markedly higher in the drip water than in the local groundwater (1007–1152 mg/l, and 276 mg/l respectively), pH was neutral (7.1–7.5). Furthermore, Ca^{2+}, Na^{+}, and K^{+} are the major cations determined, and NO_3^-, SO_4^{2-}, and Cl^- the major anions (Table VI). Concentrations of Na^{+}, K^{+}, Cl^-, NO_3^-, and boron are considerably higher in the drip water than in the local groundwater, which indicates that drip water is strongly affected by leakage from a sewage reservoir; therefore, the wetting is artificial in origin. Based on the solubility of gypsum (2.2–2.6 g/l in the temperature range 0–25 °C), and Ca^{2+} and SO_4^{2-} concentrations in drip water, the evaporation of 80 to 90% of the pore water in the overhang is necessary to initiate precipitation of gypsum.

Factors responsible for sandstone decay

The erosion rate of the overhang was compared with the: (a) freezing duration, (b) freezing duration and intensity (FDI); (c) moisture content; and (d) salt content. There is a close relationship between the erosion rate and both the freezing duration

Table VI. Concentration in drip water from overhang and local groundwater (in mg/l)

Ion	Overhang drip December 24, 2009	Overhang drip December 25, 2011	Overhang drip March 14, 2015	Čumperka Spring (Radčice)
Cl^-	179	198	128	20.0
SO_4^{2-}	240	200	162	38.0
NO_3^-	318	309	417	139
HCO_3^-	–	66	–	–
Ca^{2+}	220	132	160	42
Mg^{2+}	22	18	21	14
Na^{+}	98	89	81	6,0
K^{+}	62	53	47	11
Si	12	8	10.0	6.0
Fe	0.04	0.02	0.033	<0.005
Al	<0.05	>0.07	–	–
B	–	–	0.13	<0.005

Table V. Potential evaporation rate measured at locations E1 and E2

From	To	Number of days	E1 (mm/month)	E2 (mm/month)
May 11, 2014	May 24, 2014	13	10	8
May 24, 2014	July 2, 2014	39	13	12
July 2, 2014	August 16, 2014	45	6	10
August 16, 2014	October 5, 2014	50	6	7
October 5, 2014	December 25, 2014	81	5	5
December 25, 2014	March 14, 2015	79	5	5

and FDI. However, no relationship was found between the erosion rate and the moisture or salt content (Figure 5).

Based on our measurements and observations, the major factor responsible for the rapid erosion of the sandstone overhang is clearly the strong wetting of the sandstone pore space by seeping water in the wintertime (up to 18 wt% in the overhang, in contrast to ~5 wt% outside the overhang area). High moisture content in the pores can facilitate decay of the sandstone in several ways. First, the compressive and tensile strength decreases greatly when sandstone is wetted (cf. also Lin *et al.*, 2005; Bruthans *et al.*, 2012b, 2014). Weaker sandstone fails under lower disruptive pressures (caused by weathering) than does dry sandstone. Second, repeated wetting and drying is capable of deteriorating sandstone (Ruedrich *et al.*, 2011). Third, frost weathering strongly increases with the degree of pore saturation (Ruedrich and Siegesmund, 2006). In winter, the overhang pore space contains much more water than sandstone exposures in the nearby surroundings (Figure 3C).

The perfect match between the freeze–thaw periods and the erosion rate (Tables II and III; Figures 5A and 5B) strongly indicates that frost weathering is the major (if not the only) important weathering process operating at the studied site. The ice acts as a temporary cement, falling down of flakes is delayed until the next thaw. The highest falling intensity observed immediately after long freezing periods supports this idea. In accordance, Stark (1989) observed that longer freeze periods result in much greater destruction than the more frequent but shorter periods.

The susceptibility to frost weathering was tested with repeated cycles consisting of submerging the sandstone cubes in distilled water, followed by placing them in a freezer. Unconfined cubes lost 70% of their original weight within 62–153 cycles [mean and standard deviation (SD) 102 ± 38 cycles]. However, uniaxially loaded cubes lost 70% of their original weight after 316–384 cycles (mean and SD 347 ± 28 cycles; Figure 6). Thus, the frost weathering rate was 2–6 times higher than in the case of unconfined cubes. These results clearly document that gravity loading stress significantly affects the intensity of the frost weathering. All uniaxially loaded cubes weathered into pillars, which is also an indication of the stress effect on weathering (Figure 7A, Bruthans *et al.*, 2014).

The number of weathering cycles needed to fully disintegrate sandstone even without any load (78–187) seems to be relatively high. Nevertheless, the number of frost cycles may, in reality, be lower as the material in the overhang does not disintegrate completely, but decomposes into flakes several centimeters thick. Flakes of such a size cannot be replicated on the small cubes used in the laboratory; however, small-scale flaking was commonly observed on the cubes (Figure 7B).

Based on our monitoring (see Figure 3A) the gypsum and other salts were leached from the sandstone overhang prior to the winter period. Therefore, low salt content most probably did not affect the frost weathering. In addition, the engraving '1915', which is covered by gypsum efflorescence, shows no retreat after 100 years. In light of these observations, it is unlikely that gypsum/salt crystallization under low moisture conditions (~5 wt%) plays an important role in the rapid decay of the studied sandstone. However, gypsum and potentially occurring halite and nitratine (or other salts of Na, K-Cl, NO_3) may possibly play some role in weakening of the sandstone during the spring and summer, when evaporation dominates and salts crystallize in the sandstone pore spaces. Both halite and nitratine are deliquescent, so these salts dissolve in atmospheric moisture if the relative humidity exceeds 68–76%, dependent on their proportions (for 22 °C, Gupta *et al.*, 2015). The measurements show that the relative humidity in the overhang during the period October 1, 2013 to September 30, 2014

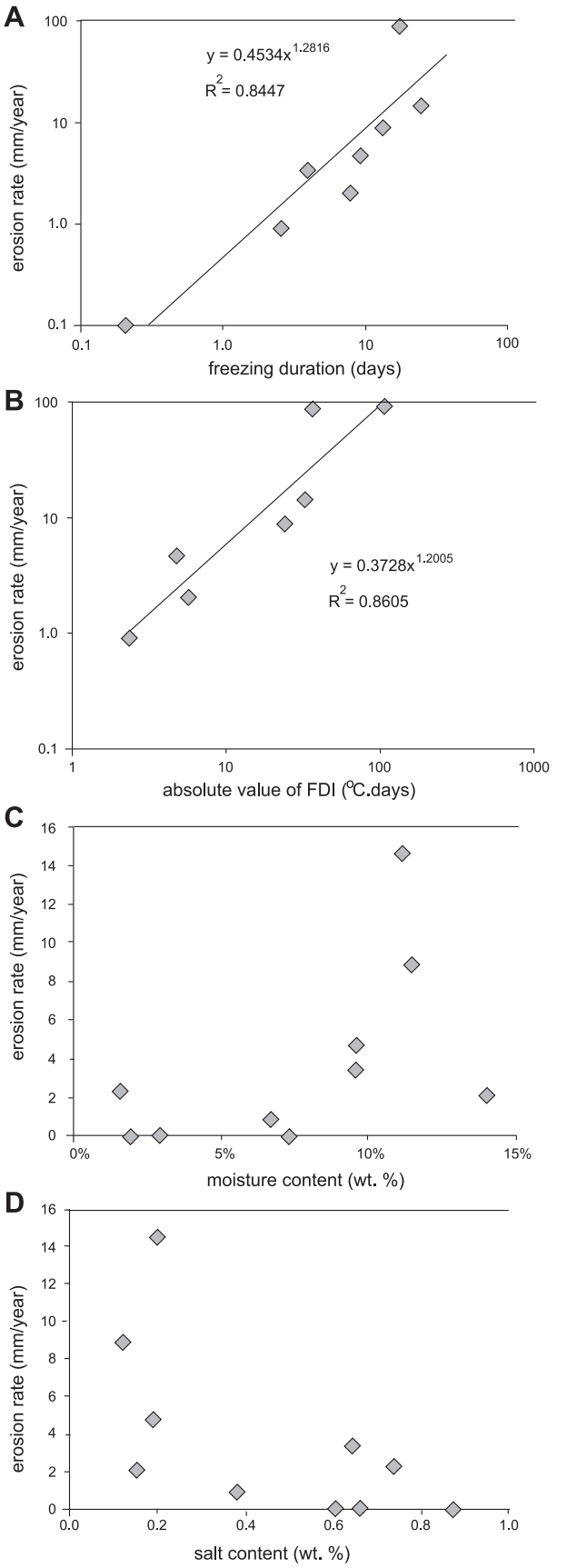

Figure 5. Relationship between erosion rate and various factors: (A) total duration of freezing; (B) absolute value of FDI – frost duration and intensity (sum of multiples of length of freezing periods and their mean temperature); (C) mean moisture content; (D) mean salt content. Erosion rates are calculated from accumulation on foil 1.

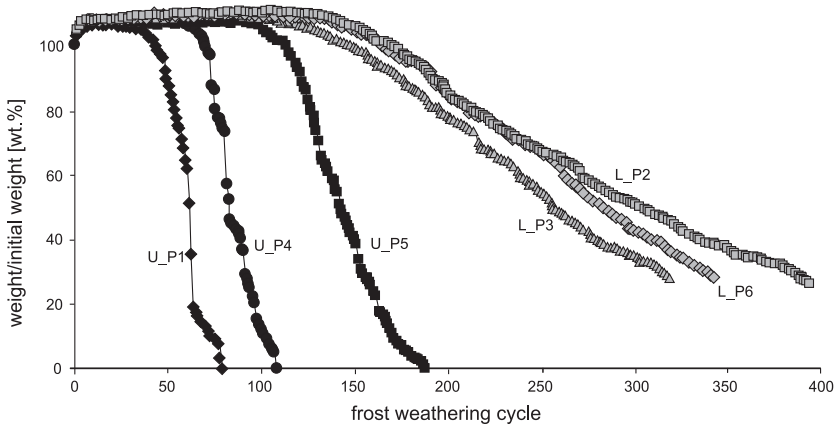

Figure 6. Frost weathering of loaded (L) and unconfined (U) cubes. Loaded cubes survived many more weathering cycles than unconfined cubes.

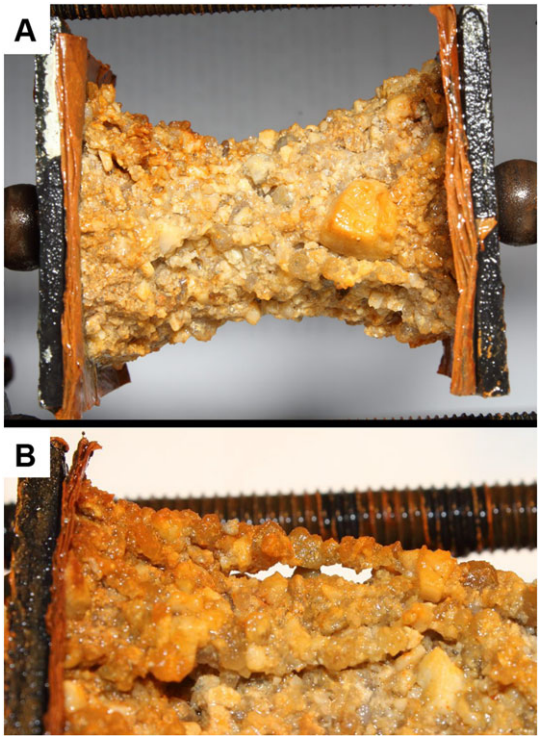

Figure 7. Laboratory frost weathering of 4 cm cubes (A) weathered into pillar, (B) small scale flaking of pillar surface. [Colour figure can be viewed at wileyonlinelibrary.com]

decreased below the 68 and 76% thresholds 175 and 201 times per year, respectively. During each such event, the halite and/or nitratine may crystallize, and dissolve once again after the event, which would considerably increase potential sandstone damage. Nitratine is reported to be 10 to 100 times more effective in degradation than gypsum (Zehnder, 1996). Halite was found to be two times more destructive than gypsum (Robinson and Williams, 2000). Additionally, the combination of gypsum with halite, and more generally with any deliquescent salt, is appreciably more destructive than either of the salts alone (Robinson and Williams, 2000; Charola *et al.*, 2007). Nevertheless, salt weathering cannot be a major weathering factor, otherwise the accumulation of the materials on the foil would occur during the first wetting of the sandstone after the summer period, and not after the thaw. The same consideration may be applied for weathering by repeated wetting and drying as well as by biodegradation.

Effects of stress on erosion rate

The erosion rate measured at the fiberglass pegs was compared with the calculated stress in the sandstone subsurface (Figure 8). The highest erosion rate (13–31 mm/yr, P3–P5) corresponds to the overhanging surface with a very low compressive stress, and even tension (stress −10 to +50 kPa). However, a low erosion rate (< 2 mm/yr) was measured at a vertical wall, with compressive stress exceeding 150 kPa (high stress, P6, P7). An erosion rate of 3 to 4 mm/yr was measured at the overhanging

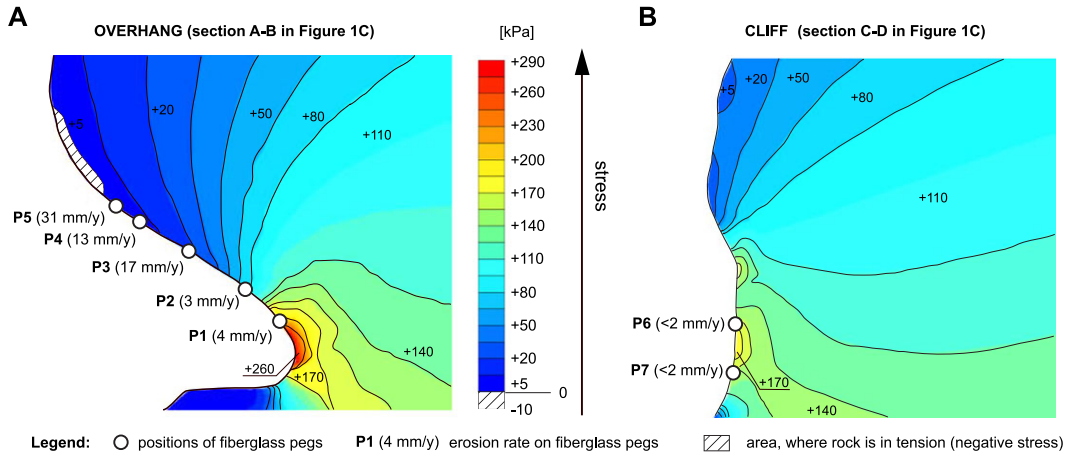

Figure 8. Numerical models showing principal stress magnitude on sections from Figure 1C. (A) Section A–B is directed across the overhang; (B) section C–D is situated across the cliff outside of the overhang area. Note that the erosion rate is decreasing with increasing stress. [Colour figure can be viewed at wileyonlinelibrary.com]

surface with a stress of 70 to 200 kPa (P1, P2). The erosion rate is thus affected by stress in the rock subsurface. Zones with low or even negative stress (tension) erode at the fastest rate; while zones with the stress exceeding 70 kPa erode at a slower rate. This is in agreement with the laboratory frost weathering experiment with the sandstone cubes, where the stress also decreased the weathering rate (Figure 6).

The magnitude of stress in the overhang subsurface is dictated by its geometry, including the overburden. The central part of overhang ceiling acts as a large protrusion (Figure 1C). For protruding parts of the sandstone massive, lower stresses are typical (Bruthans *et al.*, 2014). The protruding shape of this particular overhang is therefore strongly increasing the effect of the frost weathering. Sandstone landforms are commonly stress-controlled; this includes the overhangs lack of protruding parts, as these would have been quickly eroded (Bruthans *et al.*, 2014; Rihosek *et al.*, 2016). It is possible that the studied overhang's geometry was changed in the past during the building of a road, and the protrusion is a recent result of cutting of the western side of the overhang, which originally had a fully buttressed ceiling.

Broader consequences

Dramatic differences in the erosion rate, dependent on sandstone moisture content, can help to elucidate the development of overhangs and caves during the Holocene in the studied sandstone area (Central Europe), but also in sandstone terrains in arid temperate climate (e.g. Colorado Plateau, USA). Radiocarbon dating of sedimentary infillings at archaeological sites of sandstone overhangs and shallow caves in the northwest part of the Bohemian Cretaceous Basin has indicated that walls of these overhangs and caves recessed less than 2–5 mm/1000 years after 8–11 kyr BP (Cílek, 2007; Cílek and Žák, 2007). Radiocarbon and U-series dating of secondary carbonates demonstrated that the walls and ceilings in the north part of the Bohemian Cretaceous Basin have not recessed more than 1 mm/1000 years during the last 8 kyr BP (Bruthans *et al.*, 2012a). Similarly, the radiocarbon dating of 'fossil dung' in sandstone overhangs and caves from the Colorado Plateau have also shown that these sites were created prior to 13 kyr BP (Jennings, 1980; Davis *et al.*, 1984), and that they were not enlarged in the Holocene, except for occasional block collapses of the ceilings. It is likely that neither salt weathering nor biota can effectively disintegrate sandstone inside relatively deep and dark cavities, and that frost weathering is the most significant factor.

Our study demonstrated that sandstone, the surface of which does not measurably retreat under the present climate (rate < 0.01 mm/yr), can retreat at a rate of ~18–36 mm/yr if the pore space is nearly saturated. Similarly, increased groundwater seepage in sandstone areas can be expected in the Last Glacial period, when low temperatures greatly decreased the evapotranspiration rate. More water was left for surface flow and infiltration, as demonstrated by the high level of lakes in closed basins (Licciardi, 2001). Overhangs in Central Europe and the Colorado Plateau might thus be a result of rapid frost weathering of nearly saturated sandstone during the Last Glacial period. Seeping groundwater and possibly wind could excavate the fallen material from overhangs, and explain why there is nearly no material dated prior to 12 kyr BP in sandstone caves in both regions (Bruthans *et al.*, 2012b). The erosion of overhangs and caves followed the critical partings (Oberlander, 1977), such as clay or shale layers. The erosion of critical partings is not affected by stress, and as a consequence, the stress was not effective in decreasing the weathering rate (Bruthans *et al.*, 2014). Enlargement was strongly reduced after a change of climate in the Holocene, when relatively dry caves and overhangs became traps for sediments (cf. Cílek and Žák, 2007, p. 138).

Similar drastic changes in the erosion rate can be expected in many other situations where the climatic changes resulted in changes of the sandstone moisture content. At rare places with high moisture content the frost weathering can be relatively fast at the present time. In Adršpach (northeast Bohemian Cretaceous Basin) the frost weathering up to 240 g/m^2/yr was measured below strongly wetted sandstone blocks (unpublished). This observation does not rule out the possibility of locally relatively fast weathering/erosion by increased content of aggressive salts at the present time.

Conclusion

Characterization of those processes controlling weathering and erosion of the specific sandstone overhang near Plzeň joins together valuable data of general significance. Long-term monitoring of the parameters important for weathering was performed, and data were compared against the relevant published information. The overhang ceiling is being eroded at a mean rate of 14 mm/yr, which is unusually high compared to other measured sites elsewhere. It was revealed that 87–99% of the erosion occurs during melting after periods of freezing. Frost weathering combined with wetting weakening play major roles in the degradation of the studied sandstone overhang. Salt weathering might possibly contribute to some extent. In addition, the erosion rate is strongly affected by the geometry of the overhang and overburden, which controls the stress field in the sandstone massive. With increasing stress the erosion rate decreases as clearly demonstrated both on laboratory experiments and in the field. Exposure geometry and stress should thus be considered as important factors in weathering and erosion studies concerning sandstones (cf. Bruthans *et al.*, 2014).

The salt content in the overhang varies over the year, with the minimum in the winter, and maximum in summer or autumn. Variation in salt content inversely correlates with the oscillation of moisture content. This oscillation is adequately measurable by suction, which can therefore be used for monitoring the moisture content, with minimum damage of the rock. The results clearly show that a strong increase of the moisture content in the pores (12–18 wt% in winter) increases sandstone weathering and erosion by nearly four orders of magnitude, compared to the same material under natural moisture content (5 wt%). This finding suggests that sandstone landforms may potentially develop very rapidly if the pore space is nearly saturated by water; yet remain stable in later phases when the moisture content decreases below the critical threshold. We believe that overhangs in Central Europe, but also in other regions like in the Colorado Plateau (USA), might be the result of rapid frost weathering of nearly saturated sandstone during the Last Glacial period; and that the 'present' state is long-standing, until the next significant change of climate.

reviews of two anonymous referees and also help of editors in improving the manuscript. Hourly air temperatures were provided by the Czech Hydrometeorological Institute.

References

ASTM. 2004. *C914–95: Standard Test Method for Bulk Density and Volume of Solid Refractories by Wax Immersion*. West Conshohocken, PA: ASTM International; 188–190.

Bruthans J, Schweigstillová J, Jenč P, Churáčková Z, Bezdička P. 2012a. ^{14}C and U–series dating of speleothems in the Bohemian Paradise (Czech Republic): retreat rates of sandstone cave walls and implications for cave origin. *Acta Geodynamica et Geomaterialia* **9**: 93–108.

Bruthans J, Světlík D, Soukup J, Schweigstillová J, Válek J, Sedlackova M, Mayo AL. 2012b. Fast evolving conduits in clay-bonded sandstone: Characterization, erosion processes and significance for origin of sandstone landforms. *Geomorphology* **177–178**: 178–193.

Bruthans J, Soukup J, Vaculiková J, Filippi M, Schweigstillova J, Mayo AL, Masín D, Kletetschka G, Rihosek J. 2014. Sandstone landforms shaped by negative feedback between stress and erosion. *Nature Geoscience* **7**: 597–601.

Charola AE, Pühringer J, Steiger M. 2007. Gypsum: a review of its role in the deterioration of building materials. *Environmental Geology* **52**: 207–220.

Cílek V, Žák K. 2007. Late Glacial and Holocene sedimentation under sandstone rock shelters of Northern Bohemia (Czech Republic). In *Sandstone Landscapes*, Härtel H, Cílek V, Herben T, Jackson A, Williams R (eds). Academia: Praha; 133–138.

Cílek V. 2007. Climate, microclimate and paleoclimate of sandstone areas of Central and Northern Bohemia (Czech Republic). In *Sandstone Landscapes*, Härtel H, Cílek V, Herben T, Jackson A, Williams R (eds). Academia: Praha; 97–103.

Davis OK, Agenbroad L, Martin PS, Mead JI. 1984. The pleistocene dung blanket of Becham Cave, Utah. In *Contribution in Vertebrate Paleontology: Volume in Memorial to John E. Guilday*, Genoways HH, Dawson MR (eds). Carnegie Museum Natural History Special Publication 8. Carnegie Museum: Pittsburgh, PA; 267–282.

Dorn RI, Gordon SJ, Allen CD, Cerveny N, Dixon JC, Groom KM, Hall K, Harrison E, Mol L, Paradise TR, Sumner P, Thomson T, Turkington AV. 2013. The role of fieldwork in rock decay research: case studies from the fringe. *Geomorphology* **200**: 59–74.

Dragovich D. 1967. Flaking, a weathering process operating on cavernous rock surfaces. *Geological Society of America Bulletin* **78**: 801–804.

Gill ED. 1981. Rapid honeycomb weathering (tafoni formation) in Graywacke, S.E. Australia. *Earth Processes and Landforms* **6**: 81–83.

Gorbushina AA. 2007. Life on the rocks. *Environmental Microbiology* **9** (7): 1613–1631.

Goudie AS. 2013. *Arid and Semi-arid Geomorphology*. Cambridge University Press: Cambridge; 454 pp.

Gupta D, Kim H, Park G, Li X, Eom JH, Ro CU. 2015. Hygroscopic properties on NaCl and $NaNO_3$ mixture particles as reacted inorganic sea-salt aerosol surrogates. *Atmospheric Chemistry and Physics* **15**: 3379–3393.

Heinrichs K. 2008. Diagnosis of weathering damage on rock-cut monuments in Petra, Jordan. *Environmental Geology* **56**: 653–675.

HighScorePlus. 2011. version 3.0d, PANalytical b.v., Almelo, NL.

Huinink HP, Pel L, Kopinga K. 2004. Simulating the growth of tafoni. *Earth Surface Processes and Landforms* **29**: 1225–1233.

Imaizumi F, Nishii R, Murakami W, Daimaru H. 2015. Parallel retreat of rock slopes underlain by alternation of strata. *Geomorphology* **238**: 27–36.

JCPDS PDF2. 2004. *Sets 1-54*. International Centre for Diffraction Data: Newtown, PA.

Jennings JD. 1980. Cowboy Cave, University of Utah Anthro;pological Papers 104. University of Utah Press: Salt Lake City, UT.

Licciardi JM. 2001. Chronology of latest Pleistocene lake-level fluctuations in the pluvial Lake Chewaucan basin, Oregon, USA. *Journal of Quaternary Science* **16**(6): 545–553.

Lin ML, Jeng FS, Tsai LS, Huang TH. 2005. Wetting weakening of tertiary sandstones-microscopic mechanism. *Environmental Geology* **48**: 265–275.

Mol L. 2014. Investigations into the relationship between changes in internal moisture regimes and rock surface deterioration in cavernous sandstone features. *Earth Surface Processes and Landforms* **39**: 914–927.

Mol L, Viles HA. 2010. Geoelectric investigations into sandstone moisture regimes: Implications for rock weathering and the deterioration of San Rock Art in the Golden Gate Reserve, South Africa. *Geomorphology* **118**: 280–287.

Mol L, Viles HA. 2012. The role of rock surface hardness and internal moisture in tafoni development in sandstone. *Earth Surface Processes and Landforms* **37**: 301–314.

Mottershead DN. 1994. Spatial variations in intensity of alveolar weathering of dated sandstone structure in a coastal environment, Weston Super mare, UK. In *Rock Weathering and Landform Evolution*, Robinson DA, Williams RBG (eds). John Wiley & Sons: Chichester; 151–174.

Oberlander TM. 1977. Origin of segmented cliffs in massive sandstones of southeastern Utah. In *Geomorphology of Arid Region*s, Doehring DO (ed). Allen and Unwin: Boston, MA; 79–114.

Opluštil S, Martínek K, Tasáriová Z. 2005. Facies and architectural analysis of fluvial deposits of the Nýřany Member and the Týnec Formation (Westphalian D-Barruelian) in the Kladno-Rakovník and Pilsen basins. *Bulletin of Geosciences* **80**(1): 45–66.

Paradise TR. 2005. Petra revised: An examination of sandstone weathering research in Petra, Jordan. *Geological Society of America, Special Paper* **390**: 39–49.

Rihosek J, Bruthans J, Masin D, Filippi M, Carling GT, Schweigstillova J. 2016. Gravity-induced stress as a factor reducing decay of sandstone monuments in Petra, Jordan. *Journal of Cultural Heritage* **19**: 415–425.

Robinson DA, Williams RBG. 2000. Experimental weathering of sandstone by combinations of salts. *Earth Surface Processes and Landforms* **25**: 1309–1315.

Ruedrich J, Siegesmund S. 2006. Fabric dependence of length change behaviour induced by ice crystallization in the pore space of natural building stones. In *Heritage, Weathering and Conservation*, Fort R, Alvarez de Vuegro M, Gomez-Heras M, Vazquez-Calco C (eds). Taylor & Francis Group: London; 497–505.

Ruedrich J, Siegesmund S. 2007. Salt and ice crystallisation in porous sandstones. *Environmental Geology* **52**: 225–249.

Ruedrich J, Bartelsen T, Dohrmann R, Siegesmund S. 2011. Moisture expansion as a deterioration factor for sandstone used in buildings. *Environment and Earth Science* **63**: 1545–1564.

Siegesmund S, Snethlage R. 2011. *Stone in Architecture: Properties, Durability*. Springer Verlag: Berlin.

Stark D. 1989. Effect of length of freezing period on durability of concrete. PCA Research and Development Bulletin RD096.01T. Portland Cement Association: Skokie, IL: 9.

Steiger M, Asmussen S. 2008. Crystallization of sodium sulphate phases in porous materials: the phase diagram $Na_2SO_4{\cdot}H_2O$ and generation of stress. *Geochimica et Cosmochimica Acta* **72**: 4291–4306.

Steiger M, Charola AE, Sterflinger K. 2011. Weathering and deterioration. In *Stone in Architecture: Properties, Durability*, Siegesmund S, Snethlage R (eds). Springer Verlag: Berlin; 227–316.

Sunamura T. 1996. A physical model for the rate of coastal tafoni development. *Journal of Geology* **104**: 741–748.

Tindall JA, Kunkel JR. 1999. *Unsaturated Zone Hydrology for Scientists and Engineers*. Prentice Hall: Englewood Cliffs, NJ.

Turkington AV, Paradise TR. 2005. Sandstone weathering: a century of research and innovation. *Geomorphology* **67**: 229–253.

Viles HA. 2001. Scale issues in weathering studies. *Geomorphology* **41**: 63–72.

Viles HA. 2013. Linking weathering and rock slope instability: nonlinear perspectives. *Earth Surface Processes and Landforms* **38**: 62–70.

Viles and Goudie. 2007. Rapid salt-weathering in the coastal Namib desert: implications for landscape development. *Geomorphology* **85**(1–2): 49–62.

Vítek J. 1987. Pseudokrasové tvary v karbonských sedimentech sz. od Plzně. *Český kras* **38**: 125–127 .in Czech

Warke PA, McKinley J, Smith BJ. 2006. Variable weathering response in sandstone: Factors controlling decay sequences. *Earth Surface Processes and Landforms* **31**: 715–735.

Williams RBG, Robinson DA. 2001. Experimental frost weathering of sandstone by various combinations of salts. *Earth Surface Processes and Landforms* **26**: 811–818.

Young RW, Wray AL, Young ARM. 2009. *Sandstone Landforms*. Cambridge University Press: Cambridge.

Zehnder K. 1996. Gypsum efflorescences in the zone of rising damp. Monitoring of slow decay processes caused by crystallizing salts on wall paintings. In *Proceedings, 8th International Congress on Deterioration on Conservation of Stone*, Riederer J (ed). Möller Druck: Berlin; 1669–1678.